Deciphering Complexity in Pd–Catalyzed Cross-Couplings

George E. Clarke,[a,∥] James D. Firth,[a,∥] Lyndsay A. Ledingham,[a,∥] Chris S. Horbaczewskyj,[a] Richard Bourne,[b] Joshua T. W. Bray,[a] Poppy L. Martin,[a] Rebecca Campbell,[a] Alex Pagett,[a] Duncan J. MacQuarrie,[a] John M. Slattery,[a] Jason M. Lynam,[a] Adrian C. Whitwood,[a] Jessica Milani,[a] Sam Hart,[a] Julie Wilson,*[c] and Ian J. S. Fairlamb*[a]

[a] Department of Chemistry, University of York, Heslington, York, YO10 5DD, UK. [b] School of Chemistry, University of Leeds, Woodhouse Lane, Leeds, UK. [c] Department of Mathematics, University of York, Heslington, York, YO10 5DD, UK

∥ These authors contributed equally to this work. * Joint corresponding authors.
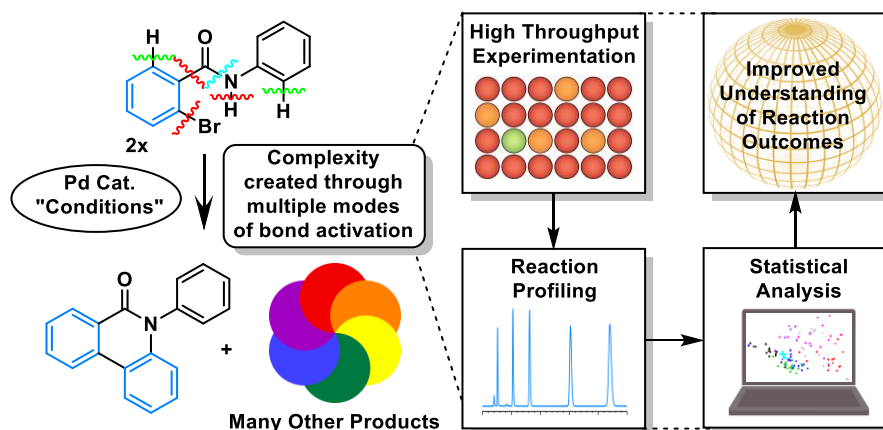
ABSTRACT: Understanding complex reaction systems and networks is critical in chemistry. While synthetic methods for the selective formation of products are highly sought after, oftentimes it is the full signature of a specific reaction, i.e. the complete profile of products/side-products, that informs mechanistic rationale and accelerates discovery chemistry. Moreover, understanding the triggers and sensitivities, under different reaction conditions, that can lead to different products assists with enhanced robustness and safety understanding. In this study we report a methodology using high-throughput experimentation methods and multivariate data analysis that can be used to take the full signature of a chemical reaction, to accelerate an understanding of the most complex reaction chemistries. To exemplify our approach, we selected a model Pd-catalyzed reaction system which forms many products – the reaction of two molecules of 2-bromo-N-phenylbenzamide, which affords primarily N-phenyl phenanthridinone. The reaction is a standout benchmark model for gaining insight on a plethora of side-products. Principal component analysis, correspondence analysis and heatmaps with hierarchical clustering have allowed us to examine the factors contributing to the variance in product distributions and show associations between solvents and reaction products. Using robust data from experiments performed with eight solvents for four different reaction times at five different temperatures, we have been able to correlate side-products to the major dominant N-phenyl phenanthridinone product, and the post-chemical modification of other side products. Complementary stoichiometric organopalladium studies allowed examination of the Pd precatalyst activation pathway, gaining insight into likely Pd reaction intermediates, particularly an oxidative addition intermediate and downstream Pd[II] intermediates.

Automated reaction screening and advanced data analysis tools are transforming the way we examine catalytic and synthetic processes. Our study offers a unique and complementary approach to revealing important reaction data on what is arguably one of the most complicated Pd catalyzed transformations known in the chemical literature.

Introduction Complex reaction networks consisting of hundreds of different species are common in many disparate types of reaction, including oxidation, pyrolysis and polymerization chemistries, with the complexity arising through the presence of many reactants or highly reactive species.[1] In contrast, the complex reaction networks of transition metal catalyzed processes originate from the nature of catalysis itself, wherein there exists an interplay of distinct elementary steps that must all occur simultaneously within a single environment. Often multiple productive catalytic cycles compete with side reactions and catalyst decomposition pathways. Furthermore, variation in (pre)catalyst, ligand, additive, solvent, and reaction stoichiometries, order of mixing and temperature (amongst other variables) can result in dramatic changes in catalytic speciation and hence reaction outcome(s).[2] Catalyst speciation adds considerable complexity, an aspect that is largely ignored in chemical synthesis, with the focus placed on the product(s) yield.[3]

Such complex reactions are often met with trepidation by synthetic chemists, with too many variables seemingly outside of their control. Indeed, most reactions under investigation in synthetic chemistry laboratories target selective formation of a single dominant product in high yield (*i.e.* an idealized outcome). However, there are opportunities to be had through embracing complexity. Firstly, complex reaction manifolds provide an opportunity for serendipitous reaction discovery, and complex reactions can often lead to the formation of unexpected high value products and new reaction chemistries.[4] Hartwig and co-workers elegantly demonstrated how complexity could be deliberately employed for discovery. Subjecting complex mixtures of reagents to potential catalysts resulted in the discovery of new reactions.[5] Secondly, developing an understanding of a complex reaction and the sensitivities to reaction conditions allows management of side-product profiles, particularly with final product purity and potential toxicity in mind. This is of vital importance in industrial process development where reliability is critical. Thirdly, studying complex reactions can lead to new mechanistic understanding through the identification of competing reaction pathways and interconnected catalytic cycles, that can be used to direct and support traditional mechanistic studies, *i.e.* hypotheses built on firm foundations involving real-world substrates and side-product profiles.

The study of complex reactions is no straight-forward task, particularly for those conducting reactions in a traditional manner, one by one, in single round-bottomed flasks.[6] However, high-throughput experimentation (HTE) is perfectly suited for the study of complex transition-metal catalyzed reactions, as it allows the rapid assessment of the effect of reaction conditions on reaction profile, under controlled conditions, whether that be in flow or batch. Indeed, over the past 20 years HTE has become a proven tool for the discovery,[4b,5] the expansion of and optimization of catalytic transformations in chemical synthesis.[7]
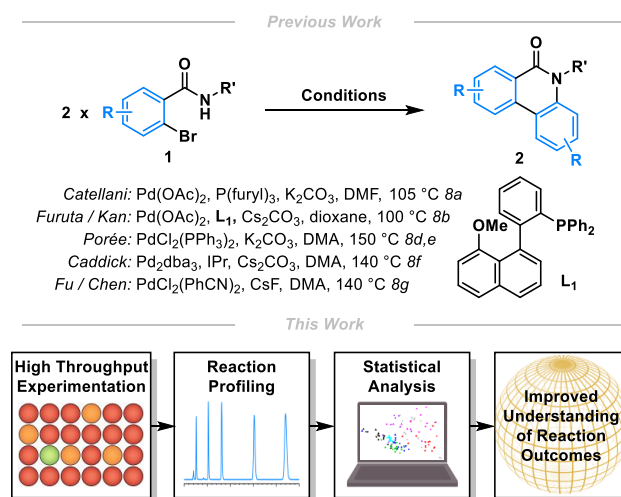
Scheme 1. Synthesis of *N*-substituted phenanthridinones **2** from 2-bromo-benzamides **1** – a formal redox-neutral dimerization and deamidation process.

Herein we report the application of HTE and multi-variate statistical analysis to the study of a complex Pd-mediated transformation. We chose to demonstrate our approach using the Pd-mediated synthesis of *N*-substituted phenanthridinones **2** from 2-bromo-benzamides **1** (Scheme 1).[8] This transformation is ideal since the starting material **1** is preconfigured to be reactively promiscuous, where there are multiple sites with capabilities for C-C and C-N bond formation and a benzamide group that can facilitate multiple bond activations.[9] This unusual reaction has been studied by several research groups and is known to generate various reactive by-products and side-products (*vide infra*). Crucially for reaction sensitivity assessment, it can be catalyzed by a wide range of catalysts and ligands (including PPh₃, P(furyl)₃, **L1** and IPr, Scheme 1), and shows solvent and base-dependent product selectivity.[8d,e] The range of Pd (pre)-catalysts, ligands, bases, solvents and temperatures (typically run at 100 °C or above) and reaction outcomes observed to date indicate that various catalytically active Pd-species and catalytic cycles are operating, but there is no detailed correlation analysis and conclusions are based on empirical evidence.

We investigate this Pd-mediated transformation from the viewpoint of complexity, rather than optimization of a major species, to facilitate a deeper and more meaningful understanding of the reaction mechanism. This comprehensive study uses a data science approach (Scheme 1) to systematically examine the extent of product and side-product formation in relation to solvent, temperature and reaction time. This approach allows a fuller understanding of the reaction network, providing new insight and advanced chemical knowledge. Moreover, information on the appearance of side-products offers opportunities in reaction discovery that might be useful from a safety perspective.
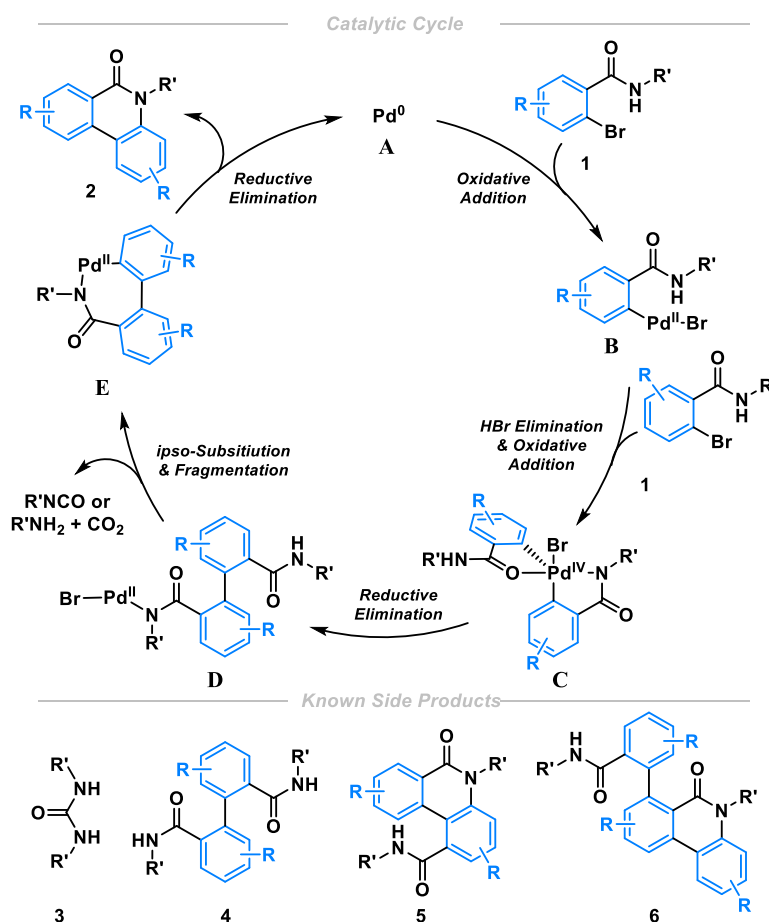
Scheme 2. Top: Catalytic cycle as proposed by Porée *et al.* – we note that discrete steps connecting **D** and **E** are required.[8e] Bottom: Reported by-products and side-products. Note: that the relationship of PPh₃ to all intermediates is not shown, but it is likely involved in various steps.

Further background into the selected reaction (1→2): Studies by Porée *et al.*[8d,e] have indicated an understanding behind the formation of phenanthridinones **2** from bromo-benzamides **1** (Scheme 2). Oxidative addition of **1** to a putative Pd^0 species **A** gives Pd^{II} intermediate **B**. Subsequent loss of HBr (base-assisted) and second oxidative addition has been proposed to result in the formation of transient Pd^{IV} species[10] **C** (based primarily on computational studies using DFT methods, conducted with and without PH$_3$ as a model phosphine ligand, and no observable transmetallation-type stoichiometric reaction involving Pd^{II} intermediates).[8e] This goes on to proceed to a key biaryl Pd^{II} intermediate **D** (which can be depicted with different Pd coordination modes), following reductive elimination. Subsequent *ipso*-substitution and elimination of reactive isocyanate and/or aniline and CO$_2$ affords 7-membered palladacycle **E**. Finally, reductive elimination generates phenanthridinone **2**.

Several potentially reactive side-products have been identified including ureas **3** (derived from isocyanate and aniline)[8a,b] as well as symmetrical biaryls **4**[8a,e] and amides **5**[8d,e] and **6**.[8a] Interestingly, ureas are known to be active ligands[11] and reagents[12] in Pd-catalyzed cross-couplings. The relationship and interplay of all these species has not been fully delineated. We recognized that HTE and data analysis of reaction outcomes offers much potential in examining further. It is of particular note that natural[13] and synthetic phenanthridinones[14] have been shown to possess a wide range of biological activities, thus a greater understanding of the reaction network would potentially aid synthesis of these useful scaffolds, allow the generation of toxicological profiles for the reaction, in addition to providing a test-bed for the development of complexity embracing experimental methodologies and data analysis.[15]

Results and Discussion

We chose to investigate the reaction of 2-bromo-*N*-phenyl benzamide **1a**, primarily because of the potential amide-directed C-H activation of the *N*-phenyl moiety. Given the ability for a range of Pd pre-catalysts and monodentate ligands to catalyze the formation of phenanthridinones **2** (Scheme 1), we planned to assess the ability of bidentate ligands to affect the transformation, particularly as their characterization in follow-on mechanistic studies (*i.e.* stoichiometric experiments with Pd) might be more facile. An initial pre-catalyst and ligand screen (see supporting information for full details) showed that 5 mol% Pd(OAc)$_2$ {formally high purity Pd$_3$(OAc)$_6$, nitrite-free}[16] and dppe, with K$_2$CO$_3$ as base in DMF[17] at 80 °C gave *N*-phenyl phenanthridinone **2a** in 58% yield (Scheme 3A). Furuta / Kan[8b] and Fu / Chen[8g] obtained **2a** in 23% and 80% yield respectively from **1a**. Crucially, for application to HTE, this reaction was found to be tolerant of air. Conducting the reaction under anhydrous and oxygen-free conditions gave a yield of **2a** which was 54%.

Since the right-hand disubstituted aryl ring in **2a** could be incorporated from either aryl group of **1a** we sought to confirm that it originates from the bromobenzene moiety (rather than the *N*-phenyl ring). As expected, use of deuterated benzamide **1a-d$_5$** gave phenanthridinone **2a-d$_5$** as a single product in 61% yield after 2 h at 130 °C. We further probed the regioselectivity of the reaction by employing methyl substituted benzamide **1b**, which afforded phenanthridinone **2b** as a single regioisomeric product in 39% yield, the structure of which was confirmed by single crystal X-ray diffraction analysis and NMR spectroscopic analysis. This molecular substitution pattern confirms[8e] the mechanism proceeds through a biaryl intermediate to **D** (Scheme 2), under our catalytic reaction conditions.
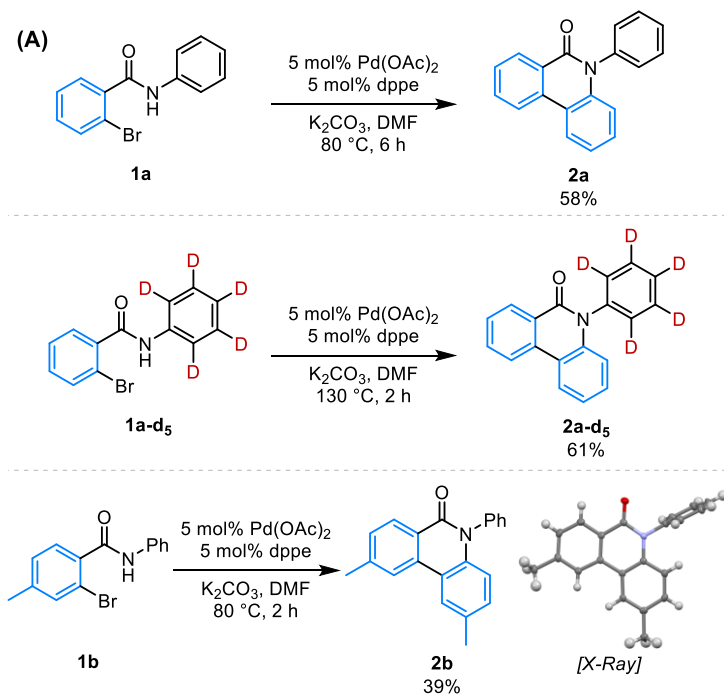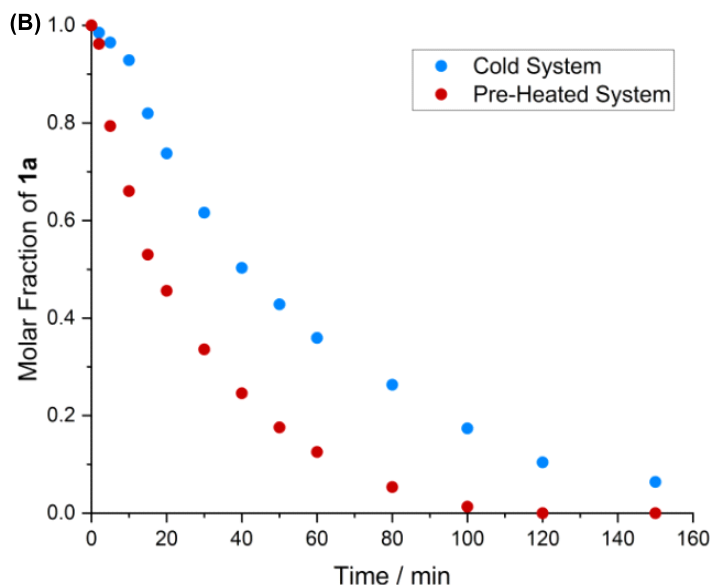
Scheme 3. A: Synthesis of *N*-phenyl phenanthridinones **2a, 2a-d₅** and **2b**. B: Reaction of **1a** at 80 °C in DMF mediated by Pd(OAc)₂/dppe (1:1, 5 mol%), showing molar fraction of **1a** (consumption) over time (GC analysis).

The reaction of **1a** mediated by Pd(OAc)₂/dppe (1:1) was monitored by GC analysis, with the consumption of **1a** assessed at 80 °C in DMF using both a cold and hot pre-activation protocol (Scheme 3B). When the reaction mixture was heated from room temperature (*ca.* 23 °C), an induction period of *ca.* 10 minutes was observed, with the reaction nearing completion (94% conversion) after 2.5 h. However, when the precatalyst mixture in DMF was heated to 80 °C for 2 min prior to addition of **1a**, the induction period was shortened (<2 min), with the reaction reaching completion within 2 h. The difference in the precatalyst activation process highlights the impact on the overall reaction time, with the pre-heating method being more effective for quantitative conversion of **1a** to products. Independent reactions between Pd(OAc)₂ and dppe showed that Pd⁰(dppe)ₙ species (*n* = 1 or 2) were formed (*vide infra*).
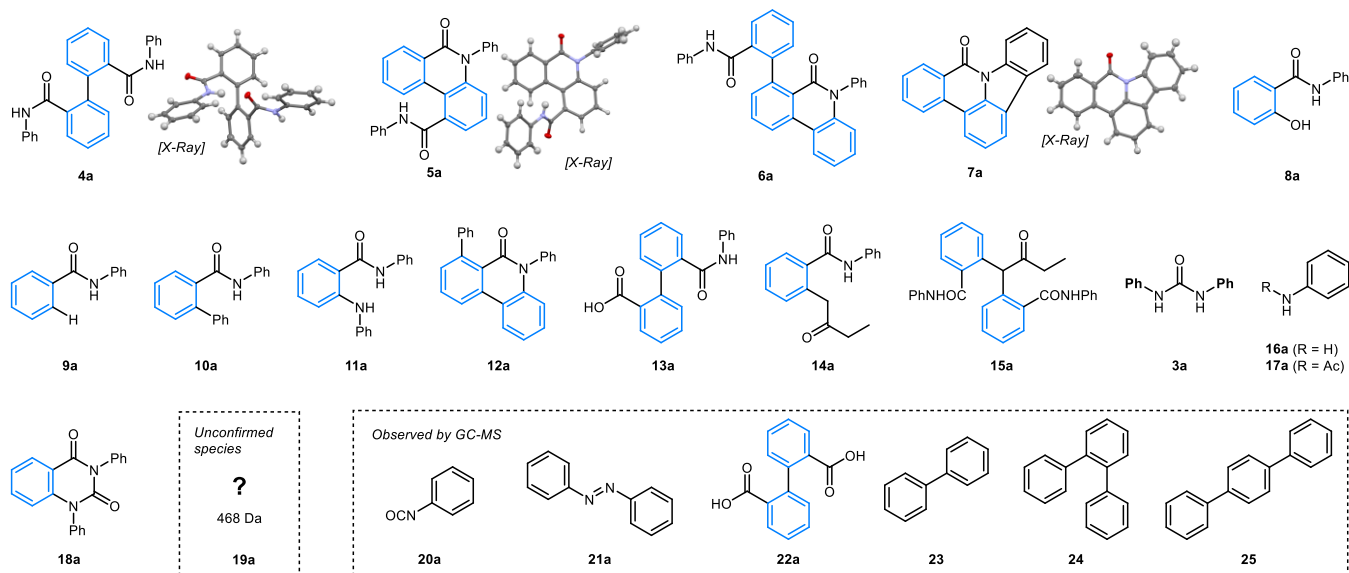
Figure 1. Reaction by-products and side-products observed by LC-MS. An unknown species **19a** is highlighted, along with additional compounds observed by GC-MS (in the inset box).

Next, a robust LC-MS method for profiling the reactions from the HTE campaign (in batch mode) was developed. Generally, we observed (by chromatographic and spectroscopic methods) that many products were formed in reaction mixtures accompanying **2a**, **2a-d₅** and **2b**, the majority of which were formed in low amounts but in significant enough quantity to warrant comprehensive profiling. This would fulfill our aspirations to gain greater understanding of this complex reaction network. Characterization of these species was achieved by LC-MS, GC-MS, flash column chromatography and preparative HPLC on the crude reaction mixtures and comparing the spectroscopic and chromatographic data with those of authentic product samples (see supporting information for full details). Through this approach we identified a total of 17 side-products and by-products of interest in the LC-MS reaction profiles (Figure 1).

Careful column chromatography resulted in the isolation and characterization of major side-products including symmetrical biaryl **4a**, isolated in ~10% yield (analogous with **4**, Scheme 2), amide **6a**,[8a] pentacycle **7a**,[18] and phenol **8a**. Amides **5a** and **6a** are analogous to compounds **5** and **6** (Scheme 2) identified by Porée[8e] and Catellani[8a] respectively. Porée *et al.* showed that phenanthridinones **5** (where R' = benzyl, methyl) were formed in presence of certain base cations and solvents,[8d,e] for which definitive conclusions could not be drawn. We examined the reaction of **1a** using Porée's pre-catalyst PdCl₂(PPh₃)₂ (5 mol%) with K₂CO₃ (3 equiv.) in dioxane at 105 °C, however **5a** was only formed in a trace quantity (by HPLC) in our hands.

Substituted phenol **8a** possibly originates from reductive elimination from a 'Ar-Pd-OH' species,[19] facilitated by the presence of residual water in the reaction medium. Interestingly, the formation of **8a** indicates the presence of hydroxide in the system, akin to the Suzuki-Miyaura cross-coupling.[20] *N*-phenyl benzamide **9a** likely occurs due to proto-dehalogenation, a side reaction that is common in Pd-catalyzed reactions in basic DMF reaction media.[21] Biaryl amide **10a**, a formal cross-coupled product, was also identified. Interestingly, experiments employing deuterated **1a-d₅** and methylated benzamide **1b** starting materials indicated that the 'new' aryl ring does not originate from 2-bromo-benzamide **1**, but instead originates from the phosphine ligand (see supporting information for full details). The reactions of phosphine ligands (*e.g.* PPh₃[22] and dppe[23]) with substrates and products at Pd is known, either via liberation of phenyl moieties and phosphido (⁻PPh₂) or phosphonium (⁺PPh₄) ions.[2]

Other side-products identified include **11a**, presumably formed through a Buchwald-Hartwig amination type reaction of 2-bromo-*N*-phenyl benzamide **1a** with aniline **16a**; arylated product **12a**, which presumably arises through amide-directed C-H arylation of phenanthridinone **2a** (as with biaryl **10a**, the 'new' aryl ring originates from the dppe ligand); and **13a**, a hydrolysis product of **4a**. Side-products **14a** and **15a** were observed when methyl ethyl ketone (MEK) was used as a solvent and likely arise through the mono- and di-α-arylation of MEK respectively.[24]

Furthermore, symmetrical urea **3a** was observed by LC-MS along with the requisite building block, aniline **16a** produced during *ipso*-substitution (**D** to **E**, Scheme 2).[8a,b] Another aniline derived side-product, acetanilide **17a**, was identified in the analytical LC-MS method. We believe that this is formed by a Pd-mediated acetylation processs.[3b] Quinazolinedione **18a**[25] could be formed through a reaction of the substrate **1a** with phenyl isocyanate **20a** (*vide infra*) and then a subsequent intramolecular amination cyclization process, or a carbonylation process.

We observed **19a** by LC-MS, which was present throughout the HTE campaign (*m/z* = 469). However, we were unable to delineate its structure (see supporting information for full details). Thus, we have treated **19a** as being an unknown species. As we demonstrate below, our approach to complex reaction analysis allows the effects of changing reaction parameters on this unknown species / contaminant to be uncovered.

Finally, we identified several species by GC-MS of the reaction mixtures that were invisible to the LC-MS method (Figure 1, bottom right). These include the expected by-product phenyl isocyanate **20a**, azobenzene **21a** from oxidative coupling of aniline, which is likely promoted by Pd nanoparticles,[26] hydrolysis product **22a** and bi- and terphenyls **23**, **24** and **25**. Whilst these species were not included in the profiling of reaction from our HTE work *vide infra*, their presence confirms the high degree of complexity of the reaction under study. Moreover, the identification of these species via GC-MS, but not LC-MS highlights that the sole use of one analysis method (which is commonplace in HTE reaction screening) ought to be viewed with some caution.

With a useful LC-MS method established, we next explored the effect of changing reaction conditions on the reaction profile using HTE. Given that most reported examples of phenanthridinone **2** syntheses use polar aprotic solvents (typically DMF and DMA) at temperatures between 100–150 °C (Scheme 1), alongside the solvent effects observed by Porée *et al.*,[8d,8e] we selected to study the effect of solvent and temperature in further detail. To this end we selected seven separate solvents {DMF, propylene carbonate, acetonitrile, *n*-butyronitrile, methyl ethyl ketone (MEK), di-*n*-butyl ether and toluene} that covered a wide range of polarities, as well as a 9:1 *n*-Bu$_2$O:DMF mixture. Furthermore, propylene carbonate,[27] and MEK[28] were selected primarily as potentially greener and less toxic alternatives. Five temperatures between 80–120 °C (10 °C intervals) were chosen, as were several reaction time-points from 1 to 8 h to provide a temporal visualization of the altering product(s) profile. Reactions were conducted at 130 °C, but significant solvent losses were noted in these experiments leading to unreliable data. We elected to perform the HTE campaign without a catalyst pre-activation step (see Scheme 3B) to avoid variability in the experimental workflow, which facilitated the range of side-products generated to be fully explored.

Reactions were performed on a Chemspeed ISYNTH robotic platform with a solid-dispensing unit[7c,d,29] to expedite reaction set-up and sampling and off-line LC-MS analysis was used to generate the reaction profile (see supporting information for full experimental details, including workflow schematic diagram). In total, 40 reactions were performed in triplicate, with sampling at four different timepoints, generating 480 reaction profiles. LC-MS alignment and peak picking were performed using automated processing (Progenesis QI)[30] and relative concentrations of the reaction constituents were obtained by normalizing the mass-ion counts over the peaks of interest (see supporting information for full details), resulting in a semi-quantification of the species of interest. This approach allows the study of the variation in amount of these (characterized and uncharacterized) species with changing reaction conditions and is simpler than developing an analytical method to show absolute quantities of all species (which would be a non-viable effort in most academic / industrial settings for reactions of this complexity).

Data analysis of reaction outcomes

Analysis of such large multidimensional datasets is difficult without multi-variate statistical analysis techniques to reduce dimensionality. To visualize the effects of reaction variables, we employed principal component analysis (PCA)[31], an unsupervised data analysis method that allows patterns in data with multiple variables to be observed in scatter plots with minimal loss of information. This is achieved by a rotation of the multi-dimensional axes, where each axis corresponds to a different variable, in our case the integrated intensities of identified peaks from LC-MS analysis. The rotation preserves the orthogonality of the axes but the first new axis, or principal component, is chosen as the direction of maximum variance in the data, the second principal component corresponds to the next most variance (orthogonal to the first) and so on. In this way, a small subset of the new axes, or principal components, provides most of the information in the data and pairwise scatter plots showing the coordinates of the observations in relation to even just the first two principal components can reveal meaningful patterns in the data. As these new axes are obtained by a rotation, each principal component is a linear combination of the original variables, or peak intensities, and the rotation matrix provides the coefficients, or loadings, of each in the linear combinations. The magnitudes of the loadings for a particular component therefore show the importance of each species to any patterns observed in the direction of that component.

We first examined data obtained at a single temperature to reduce complexity and allow the effect of time and solvent to be studied independently of temperature. At 110 °C these effects are pronounced and highlight important trends. Indeed, PCA shows clear differences between solvents (Fig. 2). For PCA plots including all times and temperatures see the supporting information. The insets show the loadings for the first two principal components (PC1 and PC2) as vectors, describing the contribution of the different compounds to the patterns seen in the corresponding scores plots.

As the variance for large peaks is greater than that for small peaks, the major products dominate the analysis and differences due to small peaks are masked unless the variables are rescaled. UV-scaling, or scaling to unit variance gives all variables equal influence on the analysis. PCA scores plots for unscaled data are shown in the supporting information. Here, differences along PC1, accounting for 97.3% of the variance in the data, are related to differences between 2-bromo-benzamide **1a**, the starting material, and product **2a**, the major product.

After scaling the data so the analysis is not dominated by the large amounts of 2-bromo-benzamide **1a** and phenanthridinone **2a**, PCA shows the distribution of side-products associated with different solvents (Fig. 2). While DMF and propylene carbonate gave the greatest amount of product **2a**, regardless of reaction time, Bu_2O led to the most **1a** remaining, with a slow but steady increase in product **2a** with increasing reaction time (Fig.2A). Other solvents, notably toluene, show a dependence on reaction time with most one-hour reactions in the centre of the plot. Bu_2O and toluene have the lowest values of most products, except perhaps products **7a**, **8a**, **9a** and **12a**. As well as the major product **2a**, DMF and propylene carbonate are likely to be associated with greater quantities of aniline **16a**, and amides **5a** and **6a**.

When considering only 2-hour reaction time points performed at different temperatures, PCA reveals similar patterns with solvent (Fig. 2B). Again Bu_2O reactions have most **1a** remaining and, except for the lowest temperature (80 °C) reactions, DMF and propylene carbonate result in the most phenanthridinone **2a**. Most solvents show increased conversion of **1a** with an increase in temperature. The greater quantities of side-products in MeCN and MEK can be seen again but outcome for both BuCN and the dual solvent system is variable. In addition to product **2a**, higher quantities of aniline **16a** and **6a** are associated with DMF and propylene carbonate, whilst Bu_2O and toluene have the lowest values. Much of the variance along PC2 is due to unusually high proportions of some compounds being recorded for a few observations, emphasized by the scaling. As the replicate experiments did not

have similar outcomes, these unusual observations could be considered outliers due to reaction sampling or analysis errors.

In order to show any trends with reaction time or temperature more clearly, outlers were removed and the analysis repeated. Outliers were determined by considering the similarity of replicates. For each set of replicates, the Euclidean distance to the centroid was calculated. The mean distance plus 1.5 standard deviations was set as a threshold and any replicates with a distance greater than this were removed. This threshold was chosen as it removed the worst outliers from each dataset without taking out too many observations. Fig. 3 shows the results for scaled data. The reaction time data now shows that MEK is most associated with greater amounts of products **10a**, **11a**, **14a**, **15a** and particularly **3a**, while MeCN, BuCN and the dual solvent system are more related with greater amounts of products **18a** and **19a** (Fig 3A). The temperature data set shows an even greater difference in the amount of these side-products for MEK and the increasing trend with temperature can be seen more clearly for MeCN, BuCN and the dual solvent system.
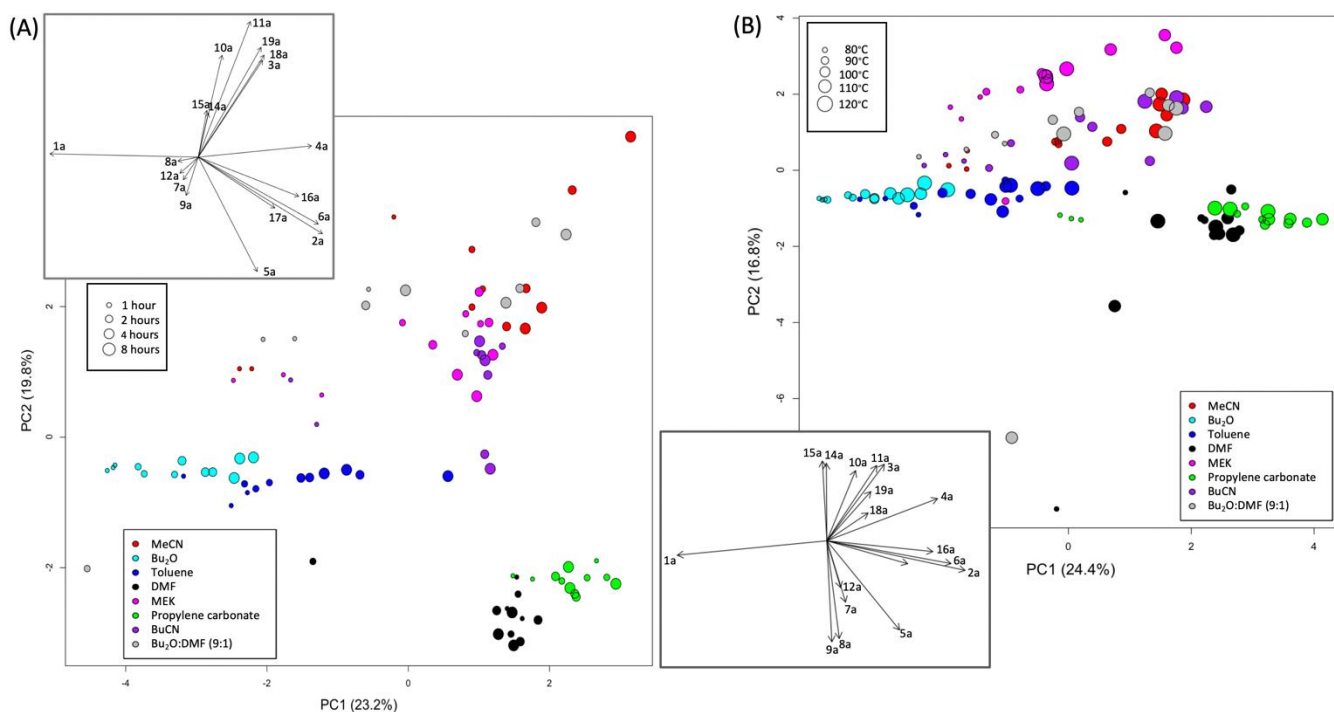
Figure 2: Scores plots for the first two principal components obtained with UV-scaled data from experiments performed in 8 different solvent systems. The plot in (A) shows experiments performed at 110 °C for 4 different reaction times whereas (B) shows 2-hour reactions performed at 5 different temperatures. The loadings, shown as vectors in the insets, indicate the contribution of the various products to the principal components.
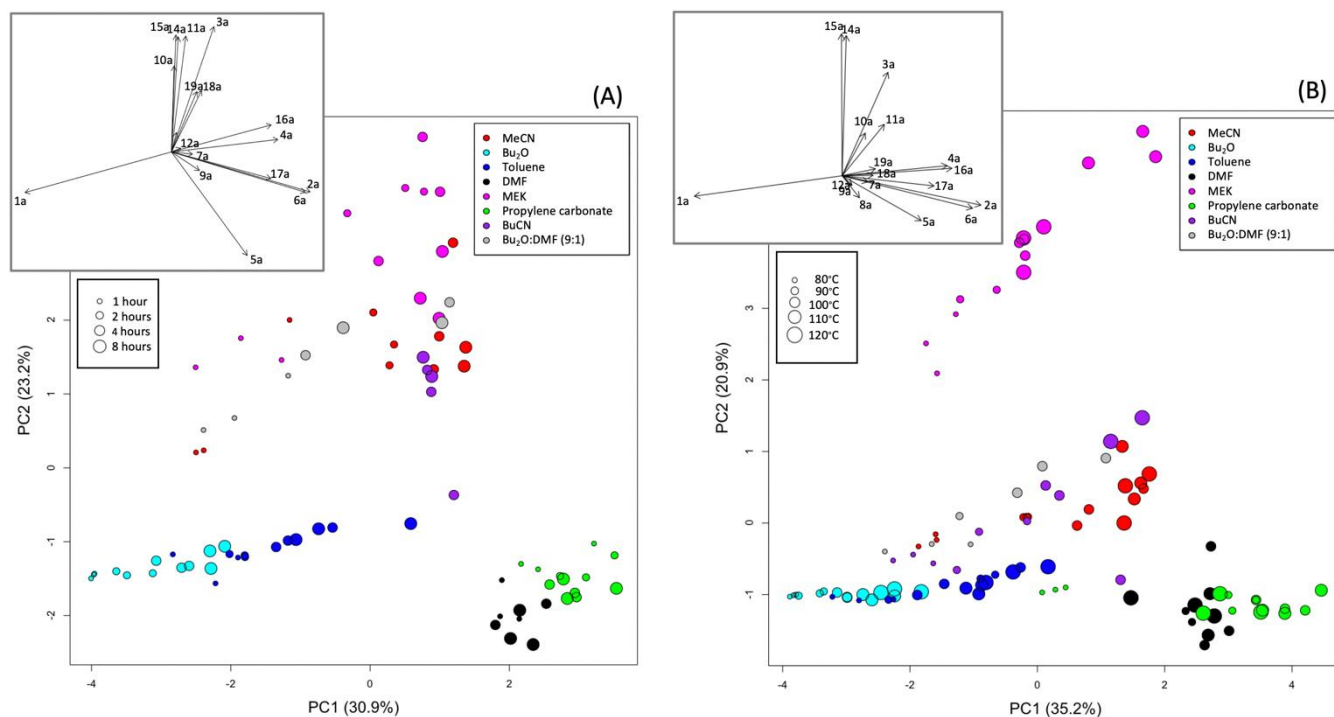
Figure 3: Scores plots for the first two principal components obtained after removing outliers from UV-scaled data from experiments performed in 8 different solvent systems. The plot in (A) shows experiments performed at 110 °C for 4 different reaction times whereas (B) shows 2-hour reactions performed at 5 different temperatures. In both cases 13 observations were removed. The loadings, shown as vectors in the insets, indicate the contribution of the various products to the principal components.
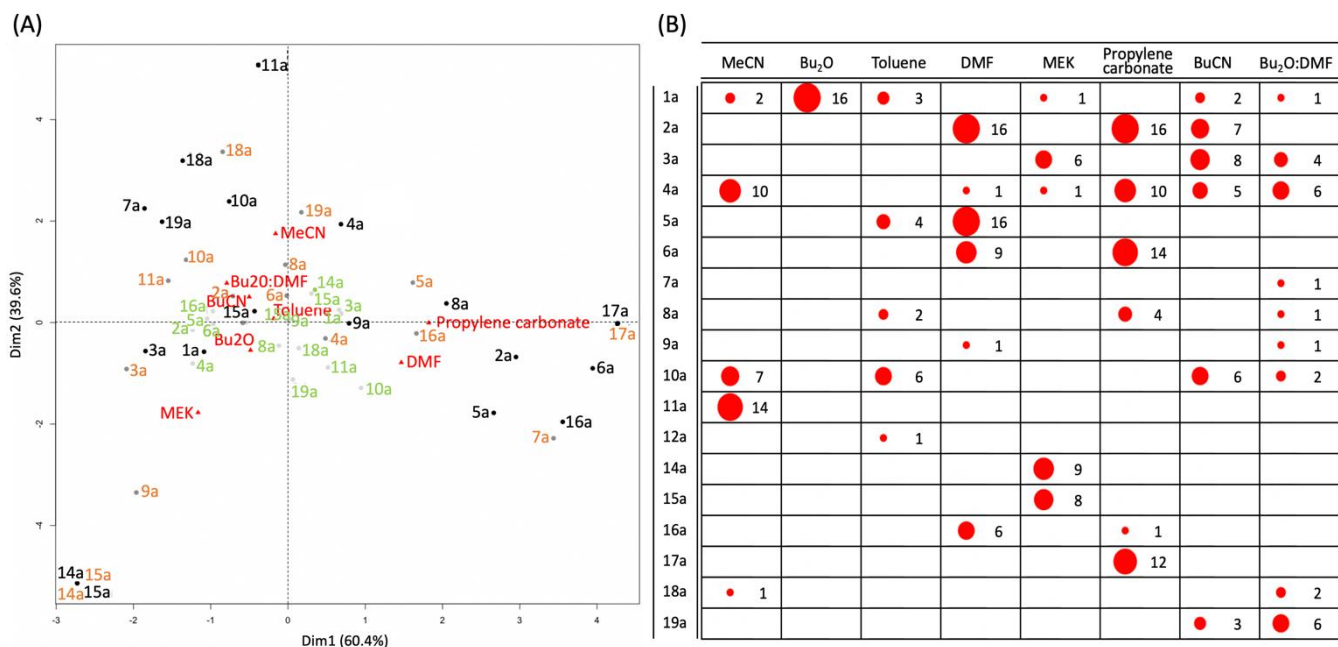
Figure 4: (A) Correspondence analysis biplot showing associations between solvents and reaction products. The number of experiments (after combining replicate analyses) with high (black), medium (orange) and low (light green) quantities for each product are used in the analysis. (B) Bubble plot showing the number of experiments with quantities above two-thirds of the range for the product by solvent. Bubble sizes are proportional to the number of experiments, also shown, where the maximum possible is 20 (*i.e.* 5 temperatures for 4 reaction times).

Figure 4B table:

	MeCN	Bu$_2$O	Toluene	DMF	MEK	Propylene carbonate	BuCN	Bu$_2$O:DMF
1a	2	16	3		1		2	1
2a				16		16	7	
3a					6		8	4
4a	10			1	1	10	5	6
5a			4	16				
6a			9			14		
7a								1
8a			2			4		1
9a				1				1
10a	7		6				6	2
11a	14							
12a			1					
14a					9			
15a					8			
16a			6			1		
17a						12		
18a	1							2
19a							3	6

Although PCA gives a good indication of the products associated with the different solvents, interpretation is complicated when several variables have similar loadings. Importantly, it is the sum of the variables that contributes to the principal component in question. For example, a lower value for side-product **6a** may be compensated for by a higher value for aniline **16a**, leading to a similar score as a higher value for product **6a** with a lower value for aniline **16a** (Fig. 2B). To determine more specific relationships between solvents and reaction products, we employed correspondence analysis (CA).[32] The median quantities were therefore calculated over replicate reactions and, for each solvent, counted the number of observations with high, medium and low quantities of each product over all temperatures and reaction times (a total of 20 for each solvent). Quantities less than a third of the full range (*i.e.* the maximum minus minimum value over all solvents) for a product were defined low, quantities between a third and two-thirds considered medium, with quantities above two-thirds of the range for product expressed as high.

The results are shown in Figure 4A. The strength of the association between solvents and reaction products depends on the distance from the origin (where the dotted lines cross) and on the angle between the vectors from the origin to the points representing the solvents and products. As in PCA, the association of DMF and propylene carbonate with high amounts of the phenanthridinone product **2a** can be seen, but here acetanilide **17a** is associated with propylene carbonate, whilst **5a** and aniline **16a** are associated with DMF. Furthermore, **6a** is associated with both propylene carbonate and, to a lesser extent, DMF.

MeCN is related to relatively high amounts of Buchwald-Hartwig product **11a**, whilst MEK is most associated with MEK α-arylation products **14a** and **15a** (as expected for the latter solvent which serves as a substrate). Other solvents, being closer to the origin, are less well discriminated.

The bubble plot in Figure 4B provides another means for data visualization. Here, only the number of experiments with high quantities are included. It can be readily seen that product **5a** is associated with reaction in DMF with 16 of the 20 reaction profiles recorded when DMF was used (5 temperatures for 4 reaction times) show relatively high

quantities of **5a**. Conversely, when the reaction is performed in propylene carbonate, no reactions exhibit high quantities of **5a**. However, 14 of the 20 reactions show high levels of **6a**. Additionally, 12 reactions show relatively high amounts of acetanilide **17a**. Again, that high amounts of α-arylation products **14a** and **15a** are only associated with MEK, which is as expected, validating our approach.
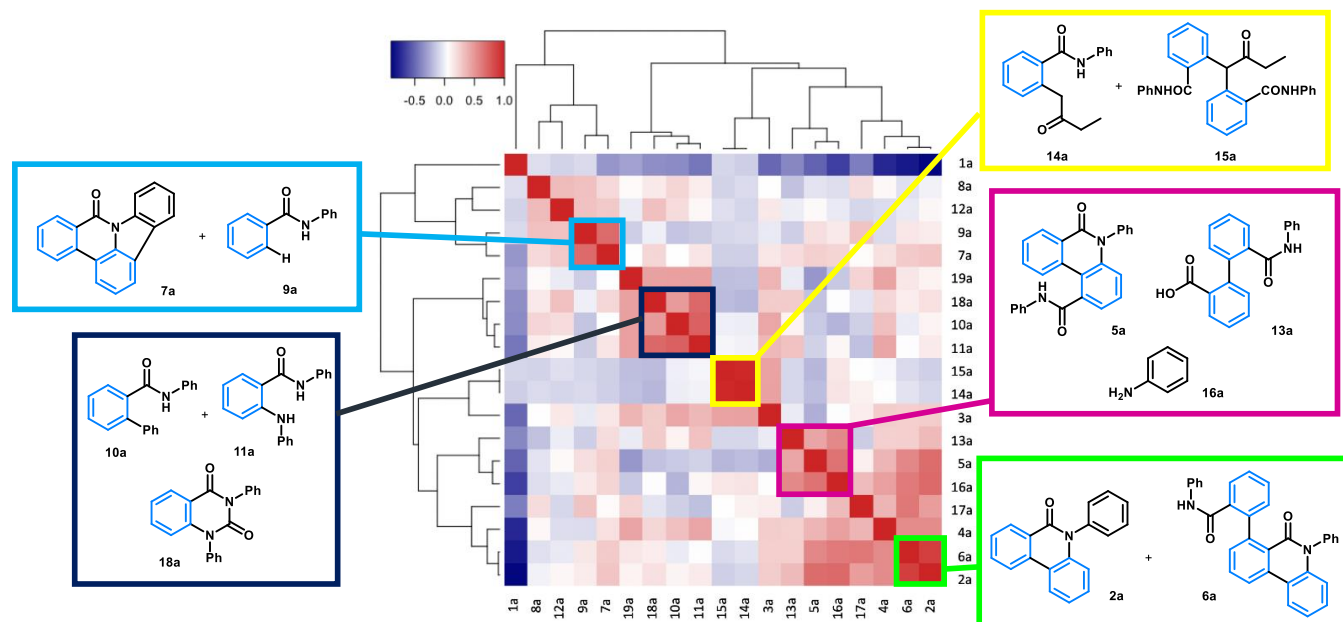
Figure 5: Heatmap showing correlations between products across reactions, including all solvents, reaction times and temperatures. Median values of replicate observations were used in the analysis. The reaction products are ordered using hierarchical clustering, resulting in the dendrograms shown in the margins, so that similar products cluster together. The map colors show the strength of correlation, as indicated by the color bar. Specific clusters of compounds are highlighted, representing selected interactions.

Heatmap analysis. To garner further mechanistic insight, we used heatmaps to visualize correlations between products. The heatmap in Figure 5 shows the strength of any correlation across all reactions between the various products. The data includes reaction solvents, temperatures and times. For example, the similarity of MEK α-arylation products **14a** and **15a** is clear from the dark red block indicating a positive correlation close to 1 (highlighted by a yellow box). The strongest negative correlations (dark blue) are between 2-bromo-benzamide **1a**, and the block of positively correlated products, aniline **16a**, biaryl diamide **4a**, **2a**-derivatized compound **6a** and phenanthridinone **2a** (the major product of the reaction). This negative correlation highlights that significant consumption of **1a** is correlated with formation of phenanthridinone **2a** and the most prevalent side-products **4a** and **6a**.

Aniline **16a** correlates with carboxylic acid **13a** (with both possibly formed from the hydrolysis of **4a**) and **5a**. Oxidative reaction of **2a** (by C-H bond activation) with urea **3a** could in principle lead to both **5a** and **16a**, leading to positive correlations.

Other blocks of positively correlated products show **7a** (oxidative cyclization product) and **9a** (reductive proto-debrominated product) grouped together. Compound **11a** (the Buchwald-Hartwig amination product) correlates with both **10a** (phenylated product) and quinazolinedione **18a**. These data correlations form the basis for mechanistic proposals (*vide infra*).

Further mechanistic analysis, supported by stoichiometric Pd chemistry. With only limited information to base our mechanistic predictions about the catalytic cycle(s) operative in this complicated chemistry, we recognized that our HTE/data analysis would be complemented by traditional stoichiometric studies involving appropriate Pd

precursor compounds. Previously proposed catalytic cycles reported by Porée *et al.*[8e] were based primarily on DFT calculations using PH_3 as a model for the PPh_3 ligand (along with an *N*-methyl substrate variant of **1a**). Such a model makes a Pd^{II}/Pd^{IV} catalytic cycle possible, in principle (Scheme 2). While higher oxidation state Pd^{IV} intermediates are experimentally feasible,[10] evidence for the stabilization of Pd^{IV} species by phosphines is relatively limited, exceptions being PPh_3[34] and transphos.[35] Indeed, the scientific community at large have often doubted Pd catalytic cycles involved phosphine-stabilized Pd^{IV} intermediates.[36] While dppe could be related to these ligands, we conducted stoichiometric ^{31}P NMR and MS experiments to better understand dppe interactions at Pd.

Amatore and Jutand showed that $Pd^0(dppe)_2$ **I'** and $Pd^0(\eta^2\text{-}dba)(dppe)$ **I-dba** are formed from the reaction of $Pd_2(dba)_3 \bullet dba$ with *n* dppe (*n* = 1 or 2) in THF.[37] In our hands, reaction of 1 equivalent of $Pd(OAc)_2$ with 1 equivalent of dppe in DMF-d_7 at 23 °C resulted in a mixture of $Pd^0(dppe)_2$ **I'** (δ 30.10 ppm; lit. δ 30.46 ppm in THF) and $Pd^{II}(dppe)(OAc)_2$ (δ 59.07 ppm; lit.[38] δ 58.9 ppm in CH_2Cl_2) being formed (Figure 6). As ligand dissociation from $Pd^0(dppe)_2$ **I'** is thought to generate the putative unsaturated (catalytic) Pd^0 species $Pd^0(dppe)$ **I**, evidence was gained by addition of dba to the mixture of $Pd^{II}(OAc)_2$/1 dppe, and cross-referencing to an authentic sample of $Pd^0(\eta^2\text{-}dba)(dppe)$ **I-dba** (δ 35.5 and 37.0 ppm, $\Delta v_{1/2}$ = 28 Hz).[37] The experiment confirmed $Pd^0(dppe)$ liberation from $Pd^0(dppe)_2$ **I'** in DMF-d_7 at 23 °C; this latter species is an observable species that could act as a catalyst reservoir.

We next assessed oxidative addition of 2-bromo-*N*-phenylbenzamide **1a** to a pre-synthesized mixture of $Pd^0(dppe)_2$ **I'** (Figure 6, red) and $Pd^0(\eta^2\text{-}dba)(dppe)$ **I-dba** (Figure 6, orange), derived from $Pd^0_2(dba)_3 \bullet dba$ and 1 dppe in DMF-d_7 at 23 °C. It was necessary to heat the mixture of **1a** with these Pd^0 species at 80 °C to give key oxidative intermediate **II** (Figure 6, yellow). Two doublets appeared at δ 41.78 and δ 59.05 ppm ($^2J_{PP}$ = 28 Hz), supporting formation of $Pd^{II}(Ar)Br(dppe)$ **II**. The ^{31}P NMR signals for oxidative addition products of this type are typically found in the δ 56–31 ppm range (in THF or DMF).[39] In our case, the molecular fragment $[M\text{-}Br]^+$ was verified by ESI-MS (+ve mode). A new singlet peak at δ 65.83 ppm (Figure 6, blue) was observed, which we attribute to key reaction intermediate **VI**, resulting from the formation of C-C bond. This proposal is supported by the detection of the sodiated pseudo-molecular ion by ESI-MS (+ve mode).

Another new species with a signal of δ 56.55 ppm (Figure 6, green) forms at 80 °C, which we tentatively assign to $Pd^{II}(dppe)(Br)_2$ **VIII** (Figure 6, green). An autoionization equilibrium was noted for the behavior of $Pd^{II}(dppe)(OAc)_2$ to give $[Pd^{II}(dppe)_2]^{2+}$ **VIII'** + "$Pd(OAc)_2$".[38] The detection of $[Pd^{II}(dppe)_2]^{2+}$ **VIII'** by ESI-MS (+ve mode) allows us to assign this signal to $Pd^{II}(dppe)(Br)_2$, **VIII** with a similar autoionization equilibrium $[Pd^{II}(dppe)_2]^{2+}$ **VIII'** + "$PdBr_2$"[38] in play. The formation of Pd black was noted at the end of this stoichiometric reaction, which is typical for these types of experiments.

Based on the complete information to hand we propose mechanistic hypotheses in Scheme 4. In terms of the catalyst activation step, we are confident that a $Pd^0(dppe)$ **I** species is generated under the reaction conditions, as the likely catalyst species (particularly in DMF), for which there are several potential reductants in the system. The generation of aniline **16a** under the working catalytic reaction conditions could assist formation of Pd^0, leading to the generation of dppe mono-oxide[40] (an alternative ligand) and acetanilide **17a**, generated through acetate transfer to aniline **16a** (see inset box for precatalyst activation in Scheme 4). We have confirmed experimentally that oxidative addition of **1a** with Pd^0 species containing dppe occurs to give **II**. From this point, a second oxidative addition of **1a** to **II** could generate Pd^{IV} species **III** (following a Porée-type mechanism[8e]). Subsequent reductive elimination generates biaryl intermediate **IV**. With the structure of **VI** being confirmed by NMR and MS, we believe that **IV** is connected by loss of two equivalents of HBr via **V** (likely base-assisted). Extrusion of phenylisocyanate **20a** affords Pd^{II} intermediate **VII**. An alternative pathway from **V**→**VII** is shown, involving a possible amide hydrolysis, liberation of CO_2 and formation of aniline **16a**. The final step involves reductive elimination from **VII** to give phenanthridinone **2a**, with concomitant regeneration of the active Pd^0 catalyst **I**.
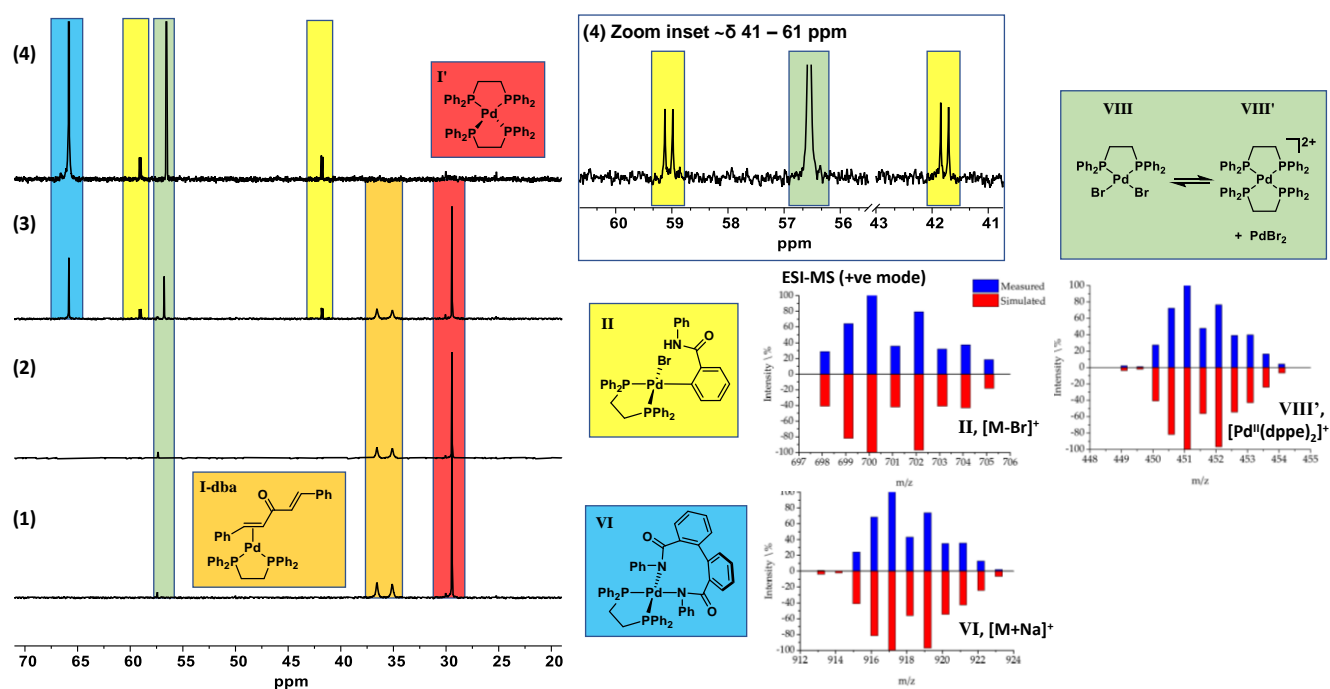
Figure 6. ^{31}P NMR (203 MHz, DMF-d_7) spectral changes and confirmation of derived (pseudo)molecular ions by ESI-MS: (1) Pd$_2$dba$_3$·CHCl$_3$ and dppe taken at rt, t = 0 mins; (2) taken after addition of 2-bromo-benzamide **1a** at rt, t = 5 mins; (3) taken after 45 minutes heating at 80 °C; (4) taken after 16 hours heating at 80 °C. We have assigned species to the five phosphorus species, cross-referenced with the ESI-MS analysis. The species at δ 57.35 is a trace product, derived from the formation of Pd^0(dba)(dppe) / Pd^0(dppe)$_2$, which is distinct to the species at δ 56.77 ppm, formed at higher temperature, assigned to PdBr$_2$(dppe) **VIII**.

Scheme 5 details the formation of major side-products **4a** (main cycle, decoordination from Pd^{II} intermediate **IV**), **5a**, **6a** and **7a**. Pentacycle **7a** is thought to arise through a formal oxidative C-H activation of phenanthridinone **2a**. Thus, reaction of Pd(dppe)Br$_2$ **VIII** with **2a** would involve formation of Pd^{II} intermediate **IX** (loss of HBr). Cyclopalladation, with loss of HBr[41] would give 6-membered ring palladacycle **X**. Finally, reductive elimination forms **7a**. The appearance of Pd(dppe)Br$_2$ **VIII** in our stoichiometric Pd experiments supports this proposal. The association of protodebrominated product **9a** with the formation of **7a** (revealed by the Heat Map analysis) suggests that **1a** is an oxidant in this competing catalytic cycle. Organohalides acting as oxidants for Pd^0→Pd^{II} is known.[42]

The heat map correlation of side-product **6a** with **2a** allows us to propose that a C-H activation process involving phenanthridinone **2a** and Pd^{II} oxidative addition intermediate **II** is likely, giving complex **XI** (detailed steps not given). Subsequent reductive elimination regenerates Pd^0 catalyst species **I**, releasing compound **6a**. Alternatively, Catellani *et al.* has suggested that compounds similar to **6** could arise by intramolecular cyclopalladation, followed by coupling with **1a** and *ipso*-substitution.[8a]
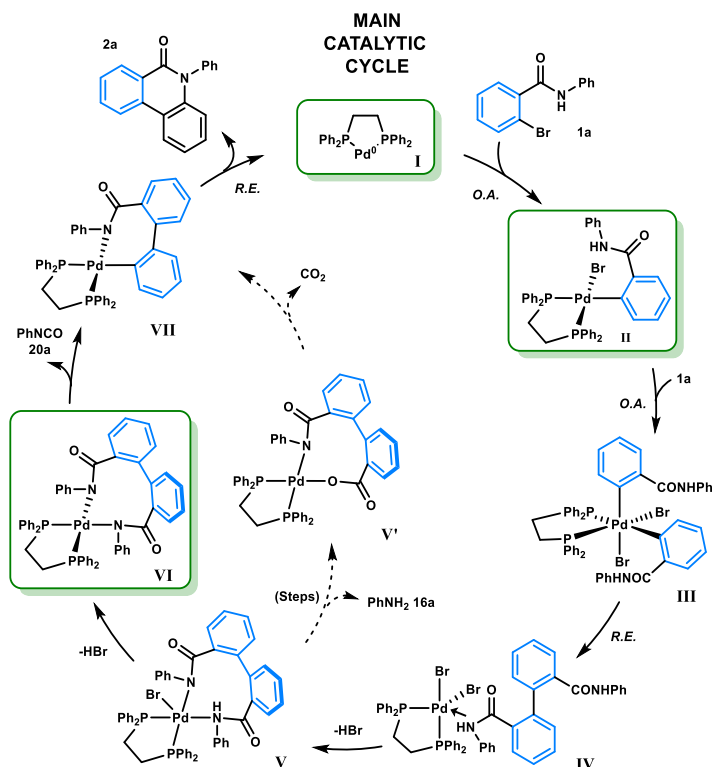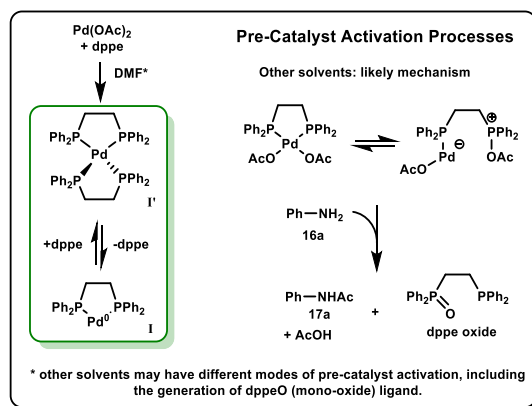
Scheme 4: Detailed catalytic cycle for the formation of phenanthridinone **2a**. Key: O.A. oxidative addition, R.E. reductive elimination. We expect all steps resulting in loss of HBr to involve base.

Key intermediate **IV** requires ligand decoordination for liberation of non-cyclized biaryl side-product **4a** and Pd(dppe)Br₂ **VIII** (observed in stoichiometric experiments, see above).

The heat map analysis revealed a correlation between **5a**, **13a** and **16a**. We propose that **5a** arises from C-H activation in **IV** to form **XII**, followed by reductive elimination. Porée[8e] *et al.* found that compounds like **5** dominated under reaction conditions in which bromine–carbonate exchange and hence, rotation around the biaryl axis, is disfavored. We acknowledge that **5a** could be formed by reaction of urea **3a** with product **2a**, for which the heat map analysis shows a strong positive correlation. Hydrolysis of **4a** likely occurs at Pd^II, thus from intermediate **IV** products carboxylic acid **13a** and aniline **16a** are formed.

The dppe ligand is a phenyl donor source that is transferred to **10a** and **12a**.[23] On the other hand, hydrolysis product **8a** likely derives from oxidative addition intermediate **II**. The heat map correlation between **10a**, **11a** and **18a** shows

that phenyl transfer from the dppe ligand is prevalent where amination occurs. Quinazolinedione **18a** formation is linked to **11a**, proposed to formed via a carbonylative process.

Scheme 5. Potential catalytic cycles for selected side-products, based on the reaction dataset correlations. We expect all steps resulting in loss of HBr to involve base.
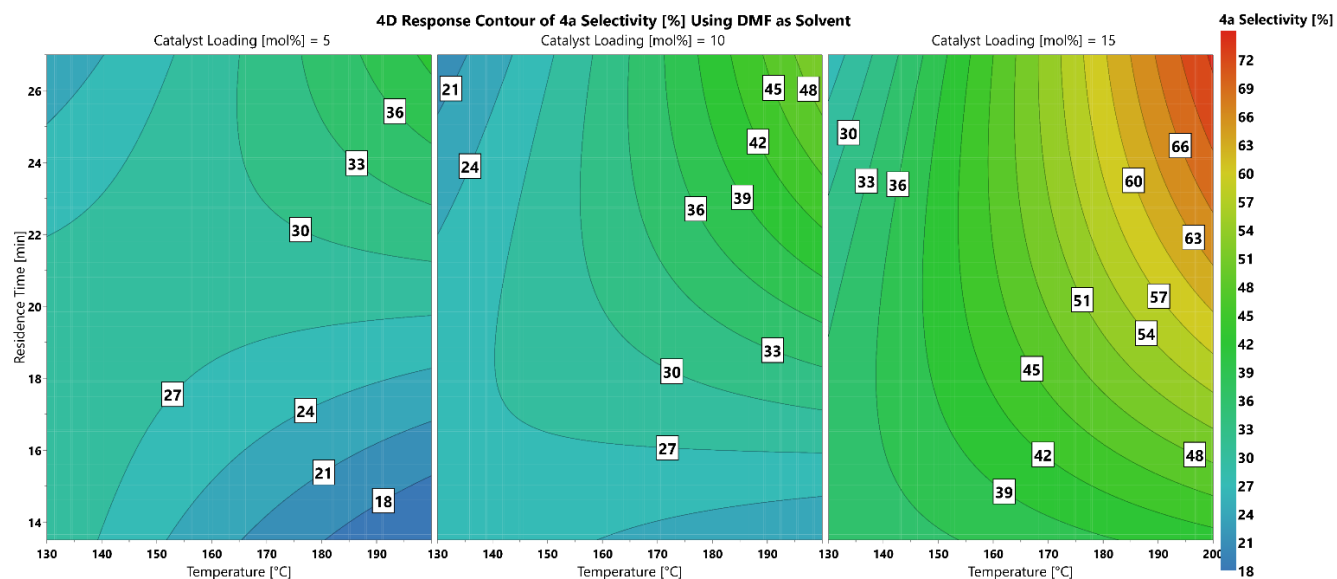
Figure 7: Contour plot of the conversion to **4a** in DMF when using 5, 10 and 15 mol% Pd(OAc)$_2$/dppe (1:1). Conversion (%) is indicated by contour lines and color.

Optimization using automated flow technology. We recognized that continuous flow platforms could be used in the study of our complex reaction chemistry.[73–77,78] We were particularly interested in whether optimization to one side product could be achieved, which batch optimization might struggle with. Our fully automated continuous flow setup allows the rapid exploration of reaction space through computer-controlled pumps, reactors and on-line HPLC.[79–83] Given the insolubility of K$_2$CO$_3$ in organic solvents, we chose to employ a heated packed bed reactor containing K$_2$CO$_3$. We investigated the effect of reaction parameters using DMF as the reaction solvent. Employing 'Design of Experiments' (DoE)[84–86] methodology (see supporting information for full details) we assessed the effect of temperature (130–200 °C), residence time (13.5–27 mins) and catalyst loading (5–15 mol%). Notably, we observed that the selectivity of the reaction **1a→2a** could be altered to favor the formation of biaryl **4a** at high temperature and catalyst loading in DMF (Figure 7). Indeed, with 15 mol% of Pd(OAc)$_2$ and dppe at 200 °C, with a residence time of 26 minutes, **4a** is formed in 70% yield. The result highlights the complementarity of the flow screening approach. For lower catalyst loadings (5 and 10 mol%), the highest conversion to **4a** is seen at high temperature and residence time. On the other hand, for both catalyst loadings, poorer conversion to **4a** was seen at both high temperature, short residence time and low temperature, high residence times. The results highlight the potential of the continuous flow platform optimization technology.

Conclusion.

Herein we have examined the highly complex Pd-catalyzed reaction of 2-bromo-*N*-phenylbenzamide **1a** to give *N*-phenyl phenanthridinone **2a** and a plethora of by-products and side-products. Automated high-throughput experimentation (HTE) methods, using both batch and flow screening technologies, have enabled the effect of temperature and solvent on the reaction profile. Principal component analysis of 480 batch reaction outcomes revealed the clear variance in starting material **1a**, product **2a** and side-product profiles based upon solvent choice. Correspondence and Heat Map (with hierarchical clustering) analysis allowed us to confidently draw associations between reaction conditions and interactions between products. This detailed reaction profiling and statistical analysis

approach has given us a fuller understanding of a complex reaction network and garnered new insight and advanced chemical knowledge. For example, the correlation between pentacycle **7a** and proto-debrominated benzamide **9a** leads us to suggest that **1a** is an oxidant in a competing catalytic cycle. Furthermore, the Pd precatalyst activation pathway has been examined using complementary stoichiometric organopalladium studies and has allowed us to gain insights into likely reaction Pd intermediates of the reaction, particularly an oxidative addition intermediate and advanced downstream Pd^{II} intermediate following activation of two molecules of 2-bromo-*N*-phenylbenzamide **1a**. Thus, this combined HTE, data rich analytical approach complemented by traditional organopalladium mechanistic studies, has allowed us to gain new insight into a highly complex Pd-mediated processes. We expect our approach in general terms, and the techniques employed, could find wide application in the field of transition metal catalysis and applied synthetic chemistry. Indeed, the full mapping out of the complexity of the reaction system (as described above), with a focus on the identification and distribution of side products, could be both a useful and rewarding point to optimize to.

ASSOCIATED CONTENT

Supporting Information

Full experimental and compound characterization details are included. We include all the details of our reaction screening experiments, and automated workflow routines.

AUTHOR INFORMATION

Corresponding Author

* Joint corresponding authors: julie.wilson@york.ac.uk; ian.fairlamb@york.ac.uk

Author Contributions

‡These authors contributed equally.

REFERENCES

(1)   Broadbelt, L. J.; Pfaendtner, J. Lexicography of Kinetic Modeling of Complex Reaction Networks. *AIChE J.* **2005**, *51*, 2112–2121.

(2)   (a) Scott, N. W. J.; Ford, M. J.; Schotes, C.; Parker, R. R.; Whitwood, A. C.; Fairlamb, I. J. S. The Ubiquitous Cross-Coupling Catalyst System 'Pd(OAc)$_2$'/2PPh$_3$ Forms a Unique Dinuclear PdI Complex: An Important Entry Point into Catalytically Competent Cyclic Pd$_3$ Clusters. *Chem. Sci.* **2019**, *10*, 7898–7906; (b) Scott, N. W. J.; Ford, M. J.; Jeddi, N.; Eyles, A.; Simon, L.; Whitwood, A. C.; Tanner, T.; Willans, C. E.; Fairlamb, I. J. S. A Dichotomy in Cross-Coupling Site Selectivity in a Dihalogenated Heteroarene: Influence of Mononuclear Pd, Pd Clusters, and Pd Nanoparticles—the Case for Exploiting Pd Catalyst Speciation. *J. Am. Chem. Soc.* **2021**, *143*, 9682–9693.

(3)   (a) Amatore, C.; Carre, E.; Jutand, A.; M'Barki, M. A. Rates and Mechanism of the Formation of Zerovalent Palladium Complexes from Mixtures of Pd(OAc)$_2$ and Tertiary Phosphines and Their Reactivity in Oxidative Additions. *Organometallics* **1995**, *14*, 1818–1826. (b) Amatore, C.; Jutand, A. Anionic Pd(0) and Pd(II) Intermediates in Palladium-Catalyzed Heck and Cross-Coupling Reactions. *Acc. Chem. Res.* **2000**, *33*, 314–321. (c) Amatore, C.; Jutand, A.; Thuilliez, A. Formation of Palladium(0) Complexes from Pd(OAc)$_2$ and a Bidentate Phosphine Ligand (Dppp) and Their Reactivity in Oxidative Addition. *Organometallics* **2001**, *20*, 3241–3249.

(4)   (a) Rulev, A. Y. Serendipity or the Art of Making Discoveries. *New J. Chem.* **2017**, *41*, 4262–4268. (b) McNally, A.; Prier, C. K.; MacMillan, D. W. C. Discovery of an α-Amino C–H Arylation Reaction Using the Strategy of Accelerated Serendipity. *Science* **2011**, *334*, 1114–1117.

(5)   (a) Robbins, D. W.; Hartwig, J. F. A Simple, Multidimensional Approach to High-Throughput Discovery of Catalytic Reactions. *Science* **2011**, *333*, 1423–1427. (b) Troshin, K.; Hartwig, J. F. Snap Deconvolution: An Informatics Approach to High-Throughput Discovery of Catalytic Reactions. *Science* **2017**, *357*, 175–181.

(6)   Allen, C. L.; Leitch, D. C.; Anson, M. S.; Zajac, M. A. The Power and Accessibility of High-Throughput Methods for Catalysis Research. *Nat. Catal.* **2019**, *2*, 2–4

(7)   (a) Isbrandt, E. S.; Sullivan, R. J.; Newman, S. G. High Throughput Strategies for the Discovery and Optimization of Catalytic Reactions. *Angew. Chem. Int. Ed.* **2019**, *58*, 7180–7191. (b) Krska, S. W.; DiRocco, D. A.; Dreher, S. D.; Shevlin, M. The Evolution of Chemical High-Throughput Experimentation To Address Challenging Problems in Pharmaceutical Synthesis. *Acc. Chem. Res.* **2017**, *50*, 2976–2985. (c) Mennen, S. M.; Alhambra, C.; Allen, C. L.; Barberis, M.; Berritt, S.; Brandt, T. A.; Campbell, A. D.; Castañón, J.; Cherney, A. H.; Christensen, M.; Damon, D. B.; Eugenio de Diego, J.; García-Cerrada, S.; García-Losada, P.; Haro, R.; Janey, J.; Leitch, D. C.; Li, L.; Liu, F.; Lobben, P. C.; MacMillan, D. W. C.; Magano, J.; McInturff, E.; Monfette, S.; Post, R. J.; Schultz, D.; Sitter, B. J.; Stevens, J. M.; Strambeanu, I. I.; Twilton, J.; Wang, K.; Zajac, M. A. The Evolution of High-Throughput Experimentation in Pharmaceutical Development and Perspectives on the Future. *Org. Process Res. Dev.* **2019**, *23*, 1213–1242. (d) Christensen, M.; Yunker, L. P. E.; Adedeji, F.; Häse, F.; Roch, L. M.; Gensch, T.; dos Passos Gomes, G.; Zepel, T.; Sigman, M. S.; Aspuru-Guzik, A.; Hein, J. E. Data-Science Driven Autonomous Process Optimization. *Commun. Chem.* **2021**, *4*, 112.

(8)   (a) Ferraccioli, R.; Carenzi, D.; Motti, E.; Catellani, M. A Simple Catalytic Synthesis of Condensed Pyridones from O-Bromoarylcarboxamides Involving Ipso Substitution via Palladacycles. *J. Am. Chem. Soc.* **2006**, *128*, 722–723. (b) Furuta, T.; Kitamura, Y.; Hashimoto, A.; Fujii, S.; Tanaka, K.; Kan, T. Efficient Synthesis of Phenanthridinone Derivatives via a Palladium-Catalyzed Coupling Process. *Org. Lett.* **2007**, *9*, 183–186. (c) Furuta, T.; Yamamoto, J.; Kitamura, Y.; Hashimoto, A.; Masu, H.; Azumaya, I.; Kan, T.;

Kawabata, T. Synthesis of Axially Chiral Amino Acid and Amino Alcohols via Additive−Ligand-Free Pd-Catalyzed Domino Coupling Reaction and Subsequent Transformations of the Product Amidoaza[5]Helicene. *J. Org. Chem.* **2010**, *75*, 7010–7013. (d) Donati, L.; Michel, S.; Tillequin, F.; Porée, F.-H. Selective Unusual Pd-Mediated Biaryl Coupling Reactions: Solvent Effects with Carbonate Bases. *Org. Lett.* **2010**, *12*, 156–158. (e) Donati, L.; Leproux, P.; Prost, E.; Michel, S.; Tillequin, F.; Gandon, V.; Porée, F.-H. Solvent/Base Effects in the Selective Domino Synthesis of Phenanthridinones That Involves High-Valent Palladium Species: Experimental and Theoretical Studies. *Chem. Eur. J.* **2011**, *17*, 12809–12819. (f) Caddick, S.; Kofie, W. Observations on the Intramolecular Heck Reactions of Aromatic Chlorides Using Palladium/Imidazolium Salts. *Tetrahedron Lett.* **2002**, *43*, 9347–9350. (g) Liu, H.; Han, W.; Li, C.; Ma, Z.; Li, R.; Zheng, X.; Fu, H.; Chen, H. Practical Synthesis of Phenanthrid-inones by Palladium-Catalyzed One-Pot C–C and C–N Coupling Reaction: Extending the Substrate Scope to o-Chlorobenzamides. *Eur. J. Org. Chem.* **2016**, 389–393.

(9)   Zheng, Q.; Liu, C.-F.; Chen, J.; Rao, G.-W. C–H Functionalization of Aromatic Amides. *Adv. Synth. Catal.* **2020**, *362*, 1406–1446.

(10)   Sehnal, P.; Taylor, R. J. K.; Fairlamb, I. J. S. Emergence of Palladium(IV) Chemistry in Synthesis and Catalysis. *Chem. Rev.* **2010**, *110*, 824–889.

(11)   (a) Cui, X.; Zhou, Y.; Wang, N.; Liu, L.; Guo, Q.-X. N-Phenylurea as an Inexpensive and Efficient Ligand for Pd-Catalyzed Heck and Room-Temperature Suzuki Reactions. *Tetrahedron Lett.* **2007**, *48*, 163–167. (b) Smith, M. R.; Kim, J. Y.; Ciufolini, M. A. Pd–Arylurea Complexes for the Heck Arylation of Crotonic and Cinnamic Substrates. *Tetrahedron Lett.* **2013**, *54*, 2042–2045. (c) Vaith, J.; Rodina, D.; Spaulding, G. C.; Paradine, S. M. Pd-Catalyzed Heteroannulation Using N-Arylureas as a Sterically Undemanding Ligand Platform. *J. Am. Chem. Soc.* **2022**, *144*, 6667–6673. (d) Cui, X.; Li, J.; Fu, Y.; Liu, L.; Guo, Q.-X. Regioselective Pd-Catalyzed Indolization of 2-Bromoanilines with Internal Alkynes Using Phosphine-Free Ligands. *Tetrahedron Lett.* **2008**, *49*, 3458–3462.

(12)   Ruiz-Castillo, P.; Buchwald, S. L. Applications of Palladium-Catalyzed C–N Cross-Coupling Reactions. *Chem. Rev.* **2016**, *116*, 12564–12649.

(13)   Bisai, V.; Saina Shaheeda, M. K.; Gupta, A.; Bisai, A. Biosynthetic Relationships and Total Syntheses of Naturally Occurring Benzo[c]Phenanthridine Alkaloids. *Asian J. Org. Chem.* **2019**, *8*, 946–969.

(14)   (a) Lugo, M.; Merrill, A. The Father, Son and Cholix Toxin: The Third Member of the DT Group Mono-ADP-Ribosyltransferase Toxin Family. *Toxins* **2015**, *7*, 2757–2772. (b) Patil, S.; Kamath, S.; Sanchez, T.; Neamati, N.; Schinazi, R. F.; Buolamwini, J. K. Synthesis and Biological Evaluation of Novel 5(H)-Phenanthridin-6-Ones, 5(H)-Phenanthridin-6-One Diketo Acid, and Polycyclic Aromatic Diketo Acid Analogs as New HIV-1 Integrase Inhibitors. *Bioorg. Med. Chem.* **2007**, *15*, 1212–1228. (c) Ishida, J.; Hattori, K.; Yamamoto, H.; Iwashita, A.; Mihara, K.; Matsuoka, N. 4-Phenyl-1,2,3,6-Tetrahydropyridine, an Excellent Fragment to Improve the Potency of PARP-1 Inhibitors. *Bioorg. Med. Chem. Lett.* **2005**, *15*, 4221–4225. (d) Dow, R. L.; Chou, T. T.; Bechle, B. M.; Goddard, C.; Larson, E. R. Identification of Tricyclic Analogs Related to Ellagic Acid as Potent/Selective Tyrosine Protein Kinase Inhibitors. *J. Med. Chem.* **1994**, *37*, 2224–2231. (e) Grese, T. A.; Adrian, M. D.; Phillips, D. L.; Shetler, P. K.; Short, L. L.; Glasebrook, A. L.; Bryant, H. U. Photochemical Synthesis of *N*-Arylbenzophenanthridine Selective Estrogen Receptor Modulators (SERMs). *J. Med. Chem.* **2001**, *44*, 2857–2860. (f) Nakamura, M.; Aoyama, A.; Salim, M. T. A.; Okamoto, M.; Baba, M.; Miyachi, H.; Hashimoto, Y.; Aoyama, H. Structural Development Studies of Anti-Hepatitis C Virus Agents with a Phenanthridinone Skeleton. *Bioorg. Med. Chem.* **2010**, *18*, 2402–2411.

(15)   Egorova, K. S.; Galushko, A. S.; Ananikov, V. P. Introducing Tox-Profiles of Chemical Reactions. *Angew. Chem. Int. Ed.* **2020**, *59,* 22296-22305.

(16)   Bajwa, S. E.; Storr, T. E.; Hatcher, L. E.; Williams, T. J.; Baumann, C. G.; Whitwood, A. C.; Allan, D. R.; Teat, S. J.; Raithby, P. R.; Fairlamb, I. J. S. On the Appearance of Nitrite Anion in [PdX(OAc)L₂] and [Pd(X)(C^N)L] Syntheses (X = OAc or NO₂): Photocrystallographic Identification of Metastable Pd(η1-ONO)(C^N)PPh₃. *Chem. Sci.* **2012**, *3*, 1656–1661.

(17)   Bernini, R.; Cacchi, S.; Fabrizi, G.; Sferrazza, A. A Simple General Approach to Phenanthridinones via Palladium-Catalyzed Intramolecular Direct Arene Arylation. *Synthesis* **2008**, 729–738.

(18)   (a) Markgraf, J. H.; Dowst, A. A.; Hensley, L. A.; Jakobsche, C. E.; Kaltner, C. J.; Webb, P. J.; Zimmerman, P. W. A Versatile Route to Benzocanthinones. *Tetrahedron* **2005**, *61*, 9102–9110. (b) Gehring, A. P.; Tremmel, T.; Bracher, F. One-Pot Conversion of 1-Bromo-β-Carboline and 1-Bromocarbazole into Pentacyclic Compounds by Suzuki Cross-Coupling Followed by Spontaneous Cyclization. *Synthesis* **2014**, *46*, 893–898.

(19)   Sergeev, A. G.; Schulz, T.; Torborg, C.; Spannenberg, A.; Neumann, H.; Beller, M. Palladium-Catalyzed Hydroxylation of Aryl Halides under Ambient Conditions. *Angew. Chem. Int. Ed.* **2009**, *48*, 7595–7599.

(20)   (a) Amatore, C.; Le Duc, G.; Jutand, A. Mechanism of Palladium-Catalyzed Suzuki–Miyaura Reactions: Multiple and Antagonistic Roles of Anionic "Bases" and Their Countercations. *Chem. Eur. J.* **2013**, *19*, 10082–10093. (b) Carrow, B. P.; Hartwig, J. F. Distinguishing Between Pathways for Transmetalation in Suzuki−Miyaura Reactions. *J. Am. Chem. Soc.* **2011**, *133*, 2116–2119.

(21)   Zawisza, A. M.; Muzart, J. Pd-Catalyzed Reduction of Aryl Halides Using Dimethylformamide as the Hydride Source. *Tetrahedron Lett.* **2007**, *48*, 6738–6742.

(22)   Goodson, F. E.; Wallow, T. I.; Novak, B. M. Mechanistic Studies on the Aryl−Aryl Interchange Reaction of ArPdL₂I (L = Triarylphosphine) Complexes. *J. Am. Chem. Soc.* **1997**, *119*, 12441–12453.

(23)   Baranano, D.; Hartwig, J. F. Carbon-Heteroatom Bond-Forming Reductive Elimination. Mechanism, Importance of Trapping Reagents, and Unusual Electronic Effects during Formation of Aryl Sulfides. *J. Am. Chem. Soc.* **1995**, *117*, 2937–2938.

(24)   (a) Crawford, S. M.; Alsabeh, P. G.; Stradiotto, M. Palladium-Catalyzed Mono-α-Arylation of Carbonyl-Containing Compounds with Aryl Halides Using DalPhos Ligands. *Eur. J. Org. Chem.* **2012**, 6042–6050. (b) Navarro, O.; Marion, N.; Oonishi, Y.; Kelly, R. A.; Nolan, S. P. Suzuki−Miyaura, α-Ketone Arylation and Dehalogenation Reactions Catalyzed by a Versatile N-Heterocyclic Carbene−Palladacycle Complex. *J. Org. Chem.* **2006**, *71*, 685–692. (c) Tan, Y.; Hartwig, J. F. Palladium-Catalyzed Amination of Aromatic C−H Bonds with Oxime Esters. *J. Am. Chem. Soc.* **2010**, *132*, 3676–3677.

(25)   Duangjan, C.; Rukachaisirikul, V.; Saithong, S.; Kaeobamrung, J. Copper-Catalyzed Domino Reaction of Carbodiimides and Benzoic Acid Derivatives for the Synthesis of Quinazolinediones. *Tetrahedron Lett.* **2018**, *59*, 3537–3540.

(26)   Cai, S.; Rong, H.; Yu, X.; Liu, X.; Wang, D.; He, W.; Li, Y. Room Temperature Activation of Oxygen by Monodispersed Metal Nanoparticles: Oxidative Dehydrogenative Coupling of Anilines for Azobenzene Syntheses. *ACS Catal.* **2013**, *3*, 478–486.

(27)   (a) Schäffner, B.; Schäffner, F.; Verevkin, S. P.; Börner, A. Organic Carbonates as Solvents in Synthesis and Catalysis. *Chem. Rev.* **2010**, *110*, 4554–4581. (b) Parker, H. L.; Sherwood, J.; Hunt, A. J.; Clark, J. H. Cyclic Carbonates as Green Alternative Solvents for the Heck Reaction. *ACS Sustain. Chem. Eng.* **2014**, *2*, 1739–1742.

(28)   Byrne, F. P.; Jin, S.; Paggiola, G.; Petchey, T. H. M.; Clark, J. H.; Farmer, T. J.; Hunt, A. J.; Robert McElroy, C.; Sherwood, J. Tools and Techniques for Solvent Selection: Green Solvent Selection Guides. *Sustain. Chem. Process.* **2016**, *4*, 7.

(29)   (a) Greenaway, R. L.; Santolini, V.; Pulido, A.; Little, M. A.; Alston, B. M.; Briggs, M. E.; Day, G. M.; Cooper, A. I.; Jelfs, K. E. From Concept to Crystals via Prediction: Multi-Component Organic Cage Pots

by Social Self-Sorting. *Angew. Chem. Int. Ed.* **2019**, *58*, 16275–16281. (b) Christensen, M.; Adedeji, F.; Grosser, S.; Zawatzky, K.; Ji, Y.; Liu, J.; Jurica, J. A.; Naber, J. R.; Hein, J. E. Development of an Automated Kinetic Profiling System with Online HPLC for Reaction Optimization. *React. Chem. Eng.* **2019**, *4*, 1555–1558. (c) Martin, M. C.; Goshu, G. M.; Hartnell, J. R.; Morris, C. D.; Wang, Y.; Tu, N. P. Versatile Methods to Dispense Submilligram Quantities of Solids Using Chemical-Coated Beads for High-Throughput Experimentation. *Org. Process Res. Dev.* **2019**, *23*, 1900–1907.

(30)   Nonlinear Dynaminc, www.nonlinear.com (accessed Feb 15, 2021).

(31)   Bro, R.; Smilde, A. K. Principal Component Analysis. *Anal. Methods* **2014**, *6*, 2812–2831.

(32) Reactions at 80 °C in DMF and 110 °C in 9:1 Bu_2O/DMF.

(33)   Hirschfeld, H. O. A Connection between Correlation and Contingency. *Math. Proc. Camb. Philos. Soc.* **1935**, *31*, 520–524.

(34)   Bayler, A.; Canty, A. J.; Skelton, B. W.; White, A. H. Organopalladium(IV) Complexes Containing Phosphine Ligands, and the Structure of the Platinum(IV) Complex $[PtMe_3(Bpy)(PPh_3)][O_3SCF_3]$ (Bpy=2,2′-Bipyridine). *J. Organomet. Chem.* **2000**, *595*, 296–299.

(35)   Gillie, A.; Stille, J. K. Mechanisms of 1,1-Reductive Elimination from Palladium. *J. Am. Chem. Soc.* **1980**, *102*, 4933–4941.

(36)   (a) Shaw, B. L. Speculations on New Mechanisms for Heck Reactions. *New J. Chem.* **1998**, *22*, 77–79. (b) Milstein, D.; Stille, J. K. Palladium-Catalyzed Coupling of Tetraorganotin Compounds with Aryl and Benzyl halides. Synthetic Utility and Mechanism. *J. Am. Chem. Soc.* **1979**, *101*, 4992–4998.

(37)   Amatore, C.; Broeker, G.; Jutand, A.; Khalil, F. Identification of the Effective Palladium(0) Catalytic Species Generated in Situ from Mixtures of $Pd(dba)_2$ and Bidentate Phosphine Ligands. Determination of Their Rates and Mechanism in Oxidative Addition. *J. Am. Chem. Soc.* **1997**, *119*, 5176–5185.

(38)   Bianchini, C.; Lee, H. M.; Meli, A.; Oberhauser, W.; Peruzzini, M.; Vizza, F. Ligand and Solvent Effects in the Alternating Copolymerization of Carbon Monoxide and Olefins by Palladium−Diphosphine Catalysis. *Organometallics* **2002**, *21*, 16–33.

(39)   (a) Mann, G.; Baranano, D.; Hartwig, J. F.; Rheingold, A. L.; Guzei, I. A. Carbon−Sulfur Bond-Forming Reductive Elimination Involving sp-, sp^2-, and sp^3-Hybridized Carbon. Mechanism, Steric Effects, and Electronic Effects on Sulfide Formation. *J. Am. Chem. Soc.* **1998**, *120*, 9205–9219. (b) Ludwig, M.; Strömberg, S.; Svensson, M.; Åkermark, B. An Exploratory Study of Regiocontrol in the Heck Type Reaction. Influence of Solvent Polarity and Bisphosphine Ligands. *Organometallics* **1999**, *18*, 970–975.

(40)   Ji, Y.; Plata, R. E.; Regens, C. S.; Hay, M.; Schmidt, M.; Razler, T.; Qiu, Y.; Geng, P.; Hsiao, Y.; Rosner, T.; Eastgate, M. D.; Blackmond, D. G. Mono-Oxidation of Bidentate Bis-Phosphines in Catalyst Activation: Kinetic and Mechanistic Studies of a Pd/Xantphos-Catalyzed C–H Functionalization. *J. Am. Chem. Soc.* **2015**, *137*, 13272–13281.

(41)   Topczewski, J. J.; Sanford, M. S. Carbon–Hydrogen (C–H) Bond Activation at Pd^{IV}: A Frontier in C–H Functionalization Catalysis. *Chem. Sci.* **2015**, *6*, 70–76.

(42)   (a) Zhao, Y.; Wang, H.; Hou, X.; Hu, Y.; Lei, A.; Zhang, H.; Zhu, L. Oxidative Cross-Coupling through Double Transmetallation: Surprisingly High Selectivity for Palladium-Catalyzed Cross-Coupling of Alkylzinc and Alkynylstannanes. *J. Am. Chem. Soc.* **2006**, *128*, 15048–15049. (b) Jin, L.; Zhao, Y.; Wang, H.; Lei, A. Palladium-Catalyzed $R(sp^3)$-Zn/R(sp)-$SnBu_3$ Oxidative Cross-Coupling. *Synthesis* **2008**, 649–654.

(43)   (a) Cambié, D.; Bottecchia, C.; Straathof, N. J. W.; Hessel, V.; Noël, T. Applications of Continuous-Flow Photochemistry in Organic Synthesis, Material Science, and Water Treatment. *Chem. Rev.* **2016**, *116*, 10276–10341. (b) Gutmann, B.; Cantillo, D.; Kappe, C. O. Continuous-Flow Technology—A Tool for the Safe Manufacturing of Active Pharmaceutical Ingredients. *Angew. Chem. Int. Ed.* **2015**, *54*, 6688–6728. (c)

Plutschack, M. B.; Pieber, B.; Gilmore, K.; Seeberger, P. H. The Hitchhiker's Guide to Flow Chemistry. *Chem. Rev.* **2017**, *117*, 11796–11893. (d) Gioiello, A.; Piccinno, A.; Lozza, A. M.; Cerra, B. The Medicinal Chemistry in the Era of Machines and Automation: Recent Advances in Continuous Flow Technology. *J. Med. Chem.* **2020**, *63*, 6624–6647. (e) Bédard, A.-C.; Adamo, A.; Aroh, K. C.; Russell, M. G.; Bedermann, A. A.; Torosian, J.; Yue, B.; Jensen, K. F.; Jamison, T. F. Reconfigurable System for Automated Optimization of Diverse Chemical Reactions. *Science* **2018**, *361*, 1220–1225. (f) Perera, D.; Tucker, J. W.; Brahmbhatt, S.; Helal, C. J.; Chong, A.; Farrell, W.; Richardson, P.; Sach, N. W. A Platform for Automated Nanomole-Scale Reaction Screening and Micromole-Scale Synthesis in Flow. *Science* **2018**, *359*, 429–434.

(44) (a) Bourne, R. A.; Skilton, R. A.; Parrott, A. J.; Irvine, D. J.; Poliakoff, M. Adaptive Process Optimization for Continuous Methylation of Alcohols in Supercritical Carbon Dioxide. *Org. Process Res. Dev.* **2011**, *15*, 932–938. (b) Holmes, N.; Akien, G. R.; Blacker, A. J.; Woodward, R. L.; Meadows, R. E.; Bourne, R. A. Self-Optimisation of the Final Stage in the Synthesis of EGFR Kinase Inhibitor AZD9291 Using an Automated Flow Reactor. *React. Chem. Eng.* **2016**, *1*, 366–371. (c) Hone, C. A.; Holmes, N.; Akien, G. R.; Bourne, R. A.; Muller, F. L. Rapid Multistep Kinetic Model Generation from Transient Flow Data. *React. Chem. Eng.* **2017**, *2*, 103–108. (d) Holmes, N.; Akien, G. R.; Savage, R. J. D.; Stanetty, C.; Baxendale, I. R.; Blacker, A. J.; Taylor, B. A.; Woodward, R. L.; Meadows, R. E.; Bourne, R. A. Online Quantitative Mass Spectrometry for the Rapid Adaptive Optimisation of Automated Flow Reactors. *React. Chem. Eng.* **2016**, *1*, 96–100. (e) Parrott, A. J.; Bourne, R. A.; Akien, G. R.; Irvine, D. J.; Poliakoff, M. Self-Optimizing Continuous Reactions in Supercritical Carbon Dioxide. *Angew. Chem. Int. Ed.* **2011**, *50*, 3788–3792.

(45) (a) Owen, M. R.; Luscombe, C.; Lai; Godbert, S.; Crookes, D. L.; Emiabata-Smith, D. Efficiency by Design: Optimisation in Process Research. *Org. Process Res. Dev.* **2001**, *5*, 308–323. (b) Weissman, S. A.; Anderson, N. G. Design of Experiments (DoE) and Process Optimization. A Review of Recent Publications. *Org. Process Res. Dev.* **2015**, *19*, 1605–1633. (c) Murray, P. M.; Bellany, F.; Benhamou, L.; Bučar, D.-K.; Tabor, A. B.; Sheppard, T. D. The Application of Design of Experiments (DoE) Reaction Optimisation and Solvent Selection in the Development of New Synthetic Chemistry. *Org. Biomol. Chem.* **2016**, *14*, 2373–2384.